

EXPERIMENTS ON FLOW INTERACTION IN A TRANSPIRATION COOLED MODEL SCRAMJET

Friedolin Strauss*, Manuel Wößner*, Matthias Weißwange*, Chiara Manfletti**, Stefan Schleichriem*

* German Aerospace Center (DLR), Institute of Space Propulsion

Langer Grund, D-74239 Hardthausen, Germany; friedolin.strauss@dlr.de

** European Space Agency (ESA), Headquarters

8-10 rue Mario Nikis, 75738 Paris Cedex 15, France; chiara.manfletti@esa.int

Abstract

Cooling experiments are performed by DLR Institute of Space Propulsion, applying a transpiration cooling system to a scramjet model combustion chamber. Nitrogen coolant is injected through different porous wall samples made of sintered stainless steel into a Mach 2.5 hot gas main flow. Different inlet conditions as well as the response of the transpiration cooling to a shock impingement caused by a 9.3° half wedge are investigated. Results show good cooling efficiency of the transpiration cooling which is not affected much by the impinging shock. A comparison with common theoretical cooling models shows their limited applicability to measurements downstream of the porous section.

Nomenclature

Ma	Mach Number [-]	u	Velocity in x-direction [m/s]
M	Molar Mass [kg mol ⁻¹]	A	Area [m ²]
T	Temperature [K]	Θ	Cooling Efficiency [-]
\dot{m}	Mass Flow [kg/s]	e	Nozzle Exit
ε	Porosity [%]	c	Coolant
c_p	Heat Capacity [J / (kg K)]	g	Main Flow (Hot Gas)
Re	Reynolds Number [-]	r	Recovery
St	Stanton Number [-]	t	Stagnation
Pr	Prandtl Number [-]	w	Wall
L	Reference Length [m]	0	Without Cooling
ν	Kinematic Viscosity [m ² s ⁻¹]	L	Referenced on Length
F	Blowing Ratio [-]	$turb$	Turbulent

1. Introduction

Worldwide research on sustainable and efficient alternatives to the propulsion systems of current aerospace vehicles has increased due to a demand for replacing toxic propellants and for modernizing existing systems for a better efficiency. In this context and facing national security challenges, ramjets with supersonic combustion - so called scramjets - among other systems are back into focus. In addition to the short fuel residence time, one of the main challenges of scramjet propulsion systems is the efficient and sufficient cooling of the engine's components. A promising cooling approach could be the method of transpiration cooling in which the coolant flows through a porous wall prior to entering the engine's main hot gas flow. By using transpiration cooling, a homogeneous and protective coolant layer of the engine wall could be achieved, thus protecting the areas with high thermal loads while keeping the engine structure at moderate temperatures. The introduction of a coolant secondary flow into the main hot gas flow can lead to phenomena like thermal choking and boundary layer combustion, which are not yet fully understood. German Aerospace Center (DLR) has developed and set up a test bench at the Institute of Space Propulsion, Lampoldshausen to investigate the applicability of transpiration cooling systems on scramjets. This test bench is used for research on cooling efficiency and flow interaction connected with this cooling approach.

The experiments presented in the publication at hand were conducted with gaseous nitrogen as inert coolant. Present and future experiments at DLR Lampoldshausen are going to use gaseous hydrogen as a more realistic, potential

reactive coolant. Carrying an inert coolant would reduce the mass average gained by using ambient air as oxidizer in any kind of scramjet propelled aerospace vehicle. Hydrogen could serve both as fuel and coolant.

As fuel residence time is a challenge, the use of flame holders and hypermixers to improve fuel / oxidizer mixing and combustion is state of the art in scramjet combustion chamber designs [1]. However it is not possible to introduce a structure like that into a supersonic flow without inducing shocks. Shock impingement on a transpiration cooling system using a reactive fuel as coolant might cause boundary layer combustion and similar phenomena. Therefore, a half wedge as a shock generator is used in DLR's experiments to create a realistic impinging shock on the transpiration cooled wall, to investigate the resulting interaction and to simulate a flame holder / hypermixer.

Several works have been published on the interaction of shocks with a transpiration cooling or film cooling system and the effects on cooling efficiency. Holden et al. [2] used 2D shock generators with 10 / 15 / 20° turning angle impinging a shock downstream of a series of holes equipped with nozzles (wall jets). They introduced a Mach 3.0 helium coolant secondary flow into a Mach 6.4 main flow with a test duration of 25 ms. This work was followed by Holden and Sweet [3] using a composite sandwich structure as porous material for creating a transpiration cooled surface. Shocks at turning angles of 5 / 7.5 / 10° were impinged on the porous surface at a free stream Mach number of 6.4 and 7.9, representing the largest Mach numbers that would be developed in a scramjet combustor. Gaseous nitrogen and helium were used as coolants being introduced at different blowing ratios, $F = (\dot{m}_c A_g) / (\dot{m}_g A_c)$. Olsen and Nowak [4] completed this analysis by using a shock generator with 2.5 / 5 / 7.5° turning angle, inducing an impinging swept-shock downstream of a film cooling slot. In the work mentioned, gaseous hydrogen and gaseous helium were used as coolants entering a Mach 6.4 nitrogen inert free stream at Mach 2.7 (hydrogen) and Mach 3.0 (helium). Interaction with a reflected expansion was also investigated.

Some authors used sintered metals to create transpiration cooling systems like the porous samples investigated in the work at hand: Meinert investigated the effect of a foreign gas transpiration on a turbulent boundary layer of a subsonic main flow ($Ma \leq 0.35$, $\dot{m} = 1.3 \text{ kg/s}$ and $298 \text{ K} \leq T_t \leq 563 \text{ K}$, see [5]). He used sintered metal samples with porosities of 20% and 30% (Sika-R 0.5 and Sika-R 5) as well as C/C material ($\varepsilon = 17\%$) similar to [6] and [7] with air, nitrogen, helium and argon as coolants for his research. His results were extended by a joint research of Meinert, Huhn, Serbest and Haidn at P8 test bench at DLR Lampoldshausen (see [8] and [9]). The stagnation temperatures in the main flow were in this case between 3520 K and 3640 K with gaseous hydrogen at ambient temperature used as coolant. Sintered stainless steel walls with porosities of 20% and 31% were used in the P8 campaign. Already in 1996 Lezuo and Haidn [10] injected gaseous hydrogen in different hot gas main flows at P8 using sintered steel walls with different porosities ([11] and [12]). Later experiments used C/C fibre ceramics in rocket combustion chambers ([6], [13]) and CMC material in scramjet model combustion chambers without flame holder or impinging shocks [14]. Song, Choi and Scotti experimented with a transpiration cooling system without main flow in [15] using tubes of sintered steel and perforated Inconel tubes. The heat flux was generated by an arc lamp generating temperatures up to 1373 K at the specimen. Pore diameters of 1.5, 3 and 5 μm were used, similar to Sika-R 1.5, Sika-R 3 and Sika-R 5.

Several publications can be found on shock-cooling system interactions in the close field of film cooling, using either similar experimental conditions or similar porous materials with the same coolants as the work at hand: Olsen et al [16] injected coolant at a Mach number of 3 and ambient temperature in a Mach 6.4 1181 K main flow, using helium as coolant. Incident shocks were created by a 0° / 5° / 10° turning angle ramp. Reference [17] introduced a coolant secondary flow with air and helium at Mach numbers 1.3 and 2.2 into a Mach 2.4 main flow, investigating how the cooling film reacts to an incident oblique shock. Results for different shock impingement positions with 6° and 15° turning angle in a Mach 2.5 nitrogen main flow were obtained by Menon [18]. A very thorough analysis of different blowing ratios of air and hydrogen into a Mach 6 main flow has been done by Alzner / Zakkay [19] interacting with the shock of a 10° turning angle shock generator. In this work, helium entered the main flow at a rearward facing step. Numerical investigations with a wedge of similar ramp angle and length, like the one used in the publication at hand, were performed by Gerlinger and Brüggemann [20]. 4° / 7° / 10° shock generators in a Mach 3.13 main flow using nitrogen, methane and hydrogen as coolants were used by Peng / Jiang in [21]. Their numerical study shows that a higher turning angle causes better mixing of the coolant with the main flow, resulting in lower cooling efficiency.

Only few publications use similar experimental conditions without shock-cooling system interaction. One of them is the work of Goldstein et al. [22], injecting air as a coolant in a Mach 2.9 air main flow using a sintered steel wall with 50% porosity. Since this porous segment has a pore size of 20 μm , it is similar to Sika-R 20 / Sika-IL 20 as it was used in the publication at hand. The cross section of the latter channel is with 63.5 x 25.4 mm similar to the channel used by DLR.

2. Experimental Setup

2.1 General Test Setup

The test bench consists of four main parts:

1. A chemical air vitiator, which burns hydrogen and oxygen to heat up pressurized air.
2. A transition section, where the geometrical shape is changed from the air vitiator's inner diameter of 135 mm to a cross section of 45 x 45 mm
3. A 45 x 45 mm Mach-2.5 supersonic nozzle
4. A transpiration cooled scramjet model combustion chamber with a plenum (reservoir) for constant coolant supply

The air vitiator (see Fig. 1) provides the necessary scramjet boundary conditions and can reach a maximum stagnation temperature of 1500 K, a maximum stagnation pressure of 25 bar and a maximum total mass flow of 5.0 kg/s. Details about the air vitiator setup, about its performance and about the reproducibility of the boundary conditions between different test runs can be found in [23] and [24].



Figure 1: Air Vitiator with Attached Supersonic Nozzle and Scramjet Model Combustion Chamber

The scramjet model combustion chamber (see Fig. 2) has a cross section of 45 x 45 mm and a length of 300 mm. In the past, similar lengths at similar Mach numbers were proven not to choke by [25], so no divergence angle was chosen. The model combustion chamber provides a cut-out in the chamber's upper wall to accommodate a porous wall section of 100 x 30 mm with a maximum thickness of 20 mm located 125 mm downstream of the chamber's intake (marked red in Fig. 3 to Fig. 5). A plenum supplies the porous section with coolant and ensures a homogeneous distribution of the coolant. An internal step in the plenum inhibits a direct blowing of coolant on the porous section in order to avoid undesired cool spots in the transpiration cooling system (see also Fig. 3 and Fig. 4).

Opposite of the porous wall section, an additional cut-out can accommodate either a 140 x 30 mm measurement plate with pressure transducers and thermocouples (see Fig. 3 for their exact locations) or a pressure tight positioning mechanism for a half-wedge shaped shock generator (9.3° ramp angle, 80 mm length, 44 mm width, marked green in Fig. 4 and 5). Two optical accesses at the side walls, covering the complete channel height can accommodate either windows for optical diagnostic methods or a 150 x 45 mm measurement plate with pressure transducers and thermocouples (see Fig. 5 for their exact locations). The optical access and the measurement plate at the side wall are covering a region 25 mm upstream up to 25 mm downstream of the porous section. 0.5 mm distance on either side between the shock generator and the optical accesses were chosen to avoid damage of the windows by thermal expansion of the wedge. Downstream of the model combustion channel no end nozzle is used in order to allow thickened boundary layers to flow off without risking choking issues too much. Further details on the general design of the scramjet model combustion chamber can be found in [23] and [24].

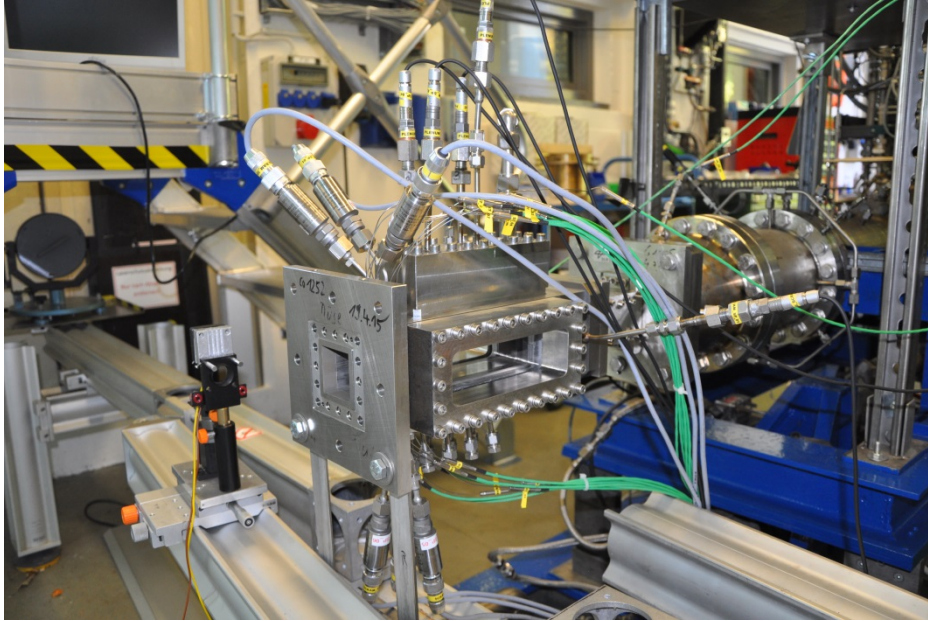


Figure 2: Scramjet Model Combustion Chamber Attached to Air Viator

2.2 Measurement and Data Acquisition Equipment

The air viator is endowed with basic measurement equipment to detect stagnation pressure, static pressure, stagnation temperature and supply pressure of hydrogen and oxygen. Control of the air viator is provided by proportional valves, which are commanded by a Siemens Simatic 7 SPS and determine predefined values for the supply pressures in order to reach the desired test points.

Basic measurement equipment of the scramjet model combustion chamber consists of a pressure transducer (*Kistler 4043A20, 0-20 bar abs.*, “SP-IN” in Fig. 4 and Fig. 5) and a thermocouple (*Thermosensors Type K*, “ST-IN” in Fig. 4 and Fig. 5) at the inlet to determine static pressure and static temperature. They are both located 35 mm downstream of the channel’s intake. Four pressure transducers (2x *Kistler 4045A50, 0-50 bar abs.* and 2x *Kistler 2043A20, 0-20 bar abs.*, “SP-PL1” to “SP-PL4” in Fig. 3 and Fig. 5) and a thermocouple (*Thermosensors Type K*, “ST-PL” in Fig. 3 and Fig. 5) measure the static temperature and the pressure distribution of the coolant in the plenum to ensure a homogeneous coolant flow along the porous wall section. Eight thermocouples in two rows with four in each row (*Thermosensors Type K*, “ST-01” to “ST-08” in Fig. 4), located 7.5 mm off the channel’s axis and 10 mm from each other) and three pressure transducers (*Measurement Specialities Type P913-G003, 0-10 bar abs.*, “SP-01” to “SP-03” in Fig. 4 and 5), located on axis and 10 mm from each other) in one row detect pressure and temperature distribution in the coolant film or coolant wake 26 to 56 mm downstream from the porous section (see Fig. 4 and 5 for details on their positions). A Coriolis mass flow metre (*Micro Motion ELITE CMF010M*) measures the coolant mass flow at the plenum’s coolant inlet.

Additional to this permanent basic measurement equipment, further sensors were used depending on the test run: eight thermocouples (*Thermosensors Type K*, “ST-09” to “ST-16” in Fig. 3 and Fig. 5) in two rows, four in each row and ten static pressure transducers (*Measurement Specialities Type P913-G003, 0-10 bar abs.*, “SP-04” to “SP-13” in Fig. 3 and Fig. 5) either in one row (lower measurement plate) or two rows, five in each row (lateral measurement plate) were connected to a lateral or lower measurement plate (see section 3 for experimental methodology and the exact sensor positions).

Optical flow investigations are performed with a Schlieren setup in Toepler’s Z-type configuration (see [26] for details). Its total length is 7.0 m with a measuring section length of 1.0 m. Two $f/10$ mirrors with 150 mm diameter are used to fold the beam path. A Cree LED with a power of 3 W and 8000 K colour temperature provides the needed light. For image acquisition a CCD cam (*The Imagine Source DFK 41B02, 1280 x 960 p, 1.2 MP, 15 fps* later replaced by *The Imagine Source DFK 33 GX174e, 1920 x 1200 p, 2.3 MP, 50 fps*) is used. With latter camera the field of view covers the complete side window section.

Data acquisition (DAQ) is provided by a *Werum 2 DAQ* system, featuring 20 HF channels for the pressure sensors and 24 LF channels for the thermocouples. HF channels are sampled at a rate of 20 kHz, whereas LF channels are sampled at 5 kHz. All thermocouples are temperature compensated by an ice box. All pressure sensors were calibrated against ambient pressure prior to each test run.

3. Methodology

Experiments were performed at four different boundary conditions provided by the air vitiator:

Table 1: Boundary Conditions Used

	Case 1	Case 2	Case 3	Case 4
Stagnation Pressure Preset [bar]	10.0	15.0	10.0	15.0
Stagnation Temperature Preset [K]	900	900	1200	1200
Mass Flow Preset [kg/s]	0.905	1.358	0.784	1.135

Three different porous materials made of sintered stainless steel were investigated (see Tab. 2 for details). For each of the porous samples, three different coolant preset pressures were determined previously in flow check tests versus ambient without a hot gas main flow. These results in various coolant mass flows and blowing ratios depend on the hot gas main flow backpressure. For reference purposes, test runs without cooling were performed at the same test points as displayed in Tab. 1.

Table 2: Characteristics of Porous Material Used

	Sika-R 150	Sika-IL 20	Sika-IL 1
Mean Pore Diameter	150 μm	20 μm	1 μm
Porosity [%] after DIN EN ISO 2738	48	43	24
Thickness [mm]	20	20	20
Material	1.4404	Inconel 600	Inconel 600

Each run was repeated three times in different configurations at a certain test point (see Tab. 3 for details on the configurations used). The excellent repeatability of the different testing points proven in [23] enables to use three different configurations at the same testing point.

Configuration 1 is used to investigate the influence of the coolant secondary flow on the cooling efficiency downstream of the porous plate whilst checking for any influence on the opposite wall, e.g. due to flow blockage (see Fig. 3). Configuration 2 makes it possible to visualize the influence of an impinging oblique shock on the transpiration cooling system and the coolant secondary flow by Schlieren method whilst measuring its influence on the cooling efficiency downstream (see Fig. 4). Configuration 3 is used for gaining the corresponding data for static pressures and static wall temperatures in the several interaction zones resulting of the impinging shock (see Fig. 5). In the experiments of the publication at hand, the half wedge was always positioned at $x = 112$ mm, when in use (see Fig. 5 for details on coordinate system and nomenclature). In this experimental campaign, 189 hot test runs have

been performed with the porous media in Tab. 1, with 144 different blowing ratios. Each test run had a testing time of ten seconds between ignition and shut down. The coolant flow started at ignition of the air viator.

Table 3: Test Configurations

	Configuration 1	Configuration 2	Configuration 3
Basic Measurement Equipment	Yes	Yes	Yes
Measurement Plate Bottom Wall	Yes	No	No
Measurement Plate Side Wall	No	No	Yes
Schlieren	Yes	Yes	No
Shock Generator	No	Yes	Yes

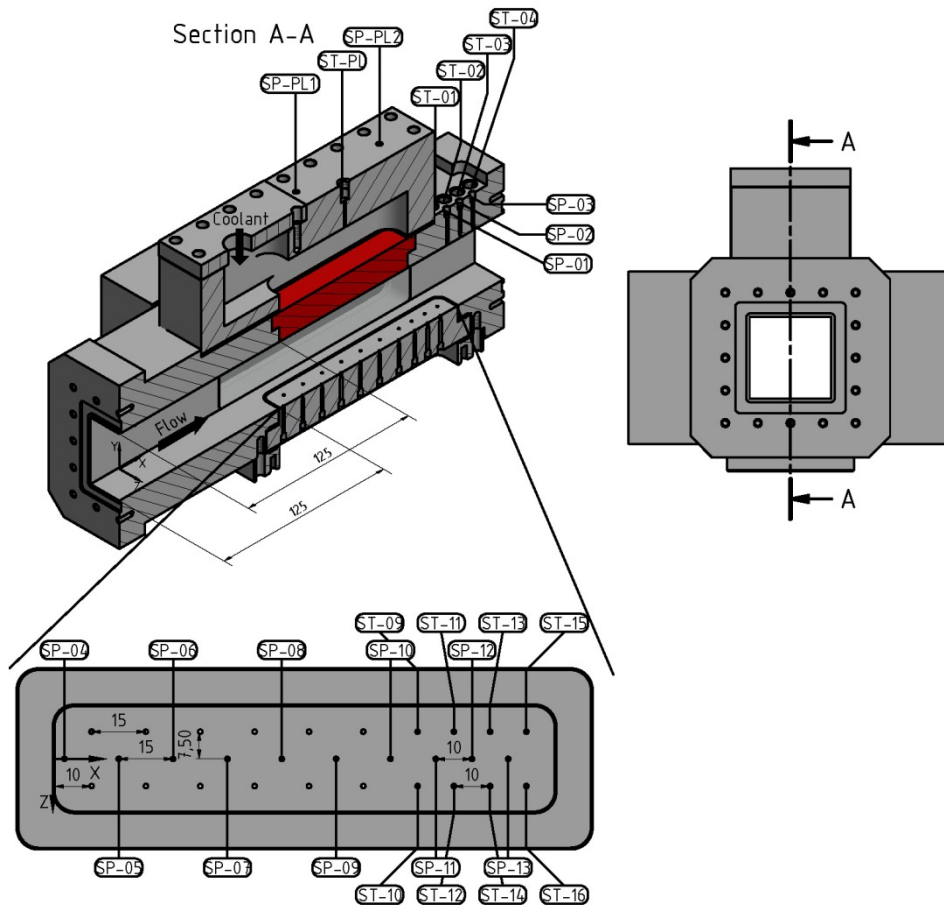


Figure 3: Test Configuration 1 of Scramjet Model Combustion Chamber

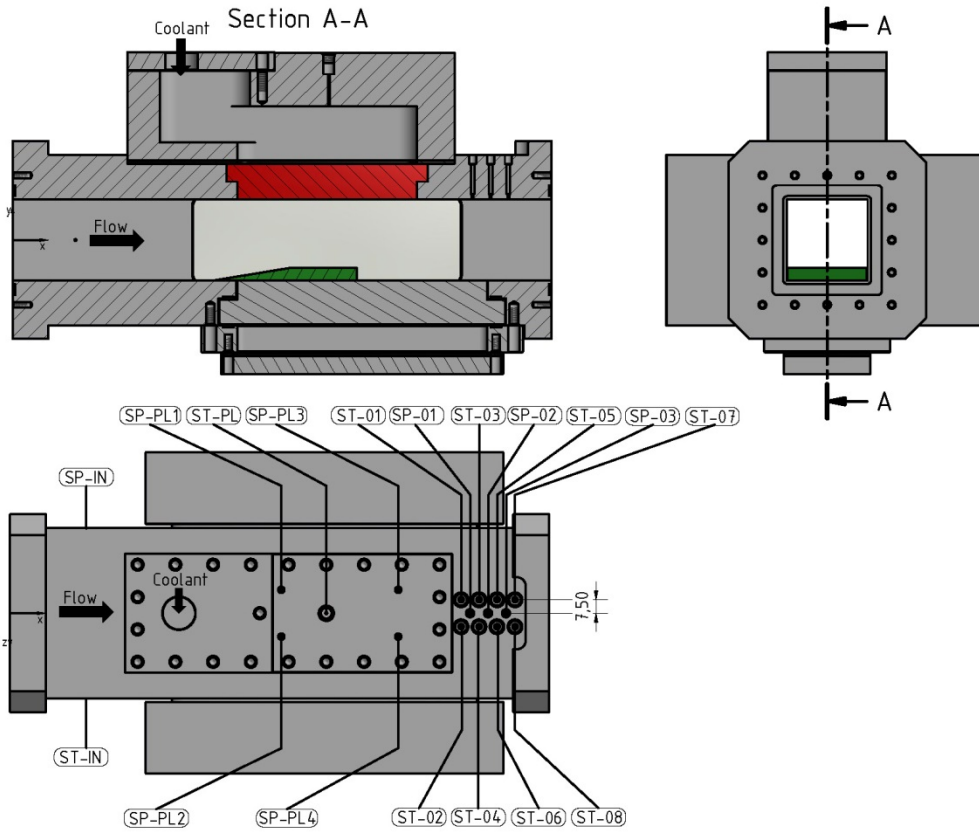


Figure 4: Test Configuration 2 of Scramjet Model Combustion Chamber and Basic Measurement Equipment

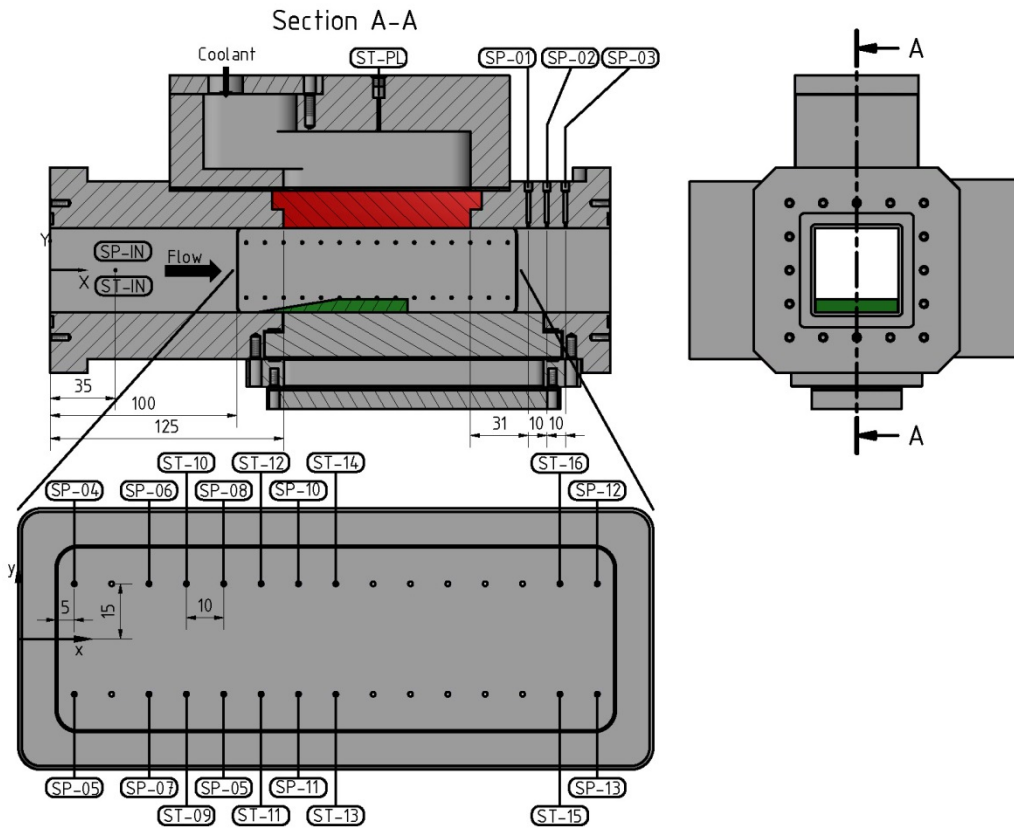


Figure 5: Test Configuration 3 of Scramjet Model Combustion Chamber

4. Results

In order to estimate the cooling efficiency of the transpiration cooling system under conditions with and without shock interaction, six different theoretical cooling models were used for comparison:

1. Eckert and Livingood (see [27])
2. Meinert, Huhn, Serbest and Haidn (see [8])
3. Fogaroli and Saydah (see [28])
4. Bartle and Leadon (see [29])
5. Kays et al. (see [30])
6. Rannie (see [31])

4.1 Cooling Efficiency According to Eckert and Livingood

For the estimation of the cooling efficiency after Eckert and Livingood [27], their equation for a transpiration cooling with turbulent flow and neglecting thermal radiation was used (see page 11 in [27] and Eq. (1)). According to their theory, the cooling efficiency yields to:

$$\Theta = \frac{T_{r,g} - T_w}{T_{r,g} - T_c} = 1 - \frac{1}{1 + \frac{\text{Re}_L^{0.1}}{2.11} \left[\exp\left(\frac{2.11}{0.037} \frac{c_{p,c}}{c_{p,g}} \text{Re}_L^{0.1} \text{Pr}_g^{2/3} F\right) - 1 \right]} \quad (1)$$

$$\text{Re}_L = \frac{u_g L}{\nu_g} \quad (2)$$

with the Reynolds number

$$\text{Pr}_g = \text{Pr}_e \quad (3)$$

and the Prandtl number

$$\text{St}_{g,0} \approx 0.037 \text{Re}_L^{-0.2} \text{Pr}_g^{-2/3} \quad (4)$$

and the Stanton number without cooling

$$\text{and the blowing ratio} \quad F = \frac{\dot{m}_c A_g}{\dot{m}_g A_c} \quad (5)$$

The hot gas main mass flow \dot{m}_g in Eq. (5) is determined via the values measured at the air vitiator. The coolant mass flow \dot{m}_c in Eq. (5) is determined via the value measured by the Coriolis mass flow meter. A_g indicates the cross section area of the channel and A_c the area of the porous wall segment. The velocity u_g in Eq. (2) can be determined out of the air vitiator data, as well as the Prandtl number Pr_g in Eq. (3). L in Eq. (2) was chosen to be the length of the porous wall section.

4.2 Cooling Efficiency According to Meinert et al.

For the estimation of the cooling efficiency after Meinert, Huhn, Serbest and Haidn [8] Eq. 6 in combination with Eq. 7 and 8 were used. The Stanton number without cooling $\text{St}_{g,0}$ in our experiments was determined after Eq. (4)

$$\Theta = \frac{T_{r,g} - T_w}{T_{r,g} - T_c} = 1 - \frac{1}{1 + \frac{c_{p,c}}{c_{p,g}} \frac{1}{k_M^* k_T^*} \left[\exp\left(\frac{F}{\text{St}_{g,0}} k_M^* k_T^*\right) - 1 \right]} \quad (6)$$

$$k_M^* = \left(\frac{M_g}{M_c} \right)^{0.6} \quad (7)$$

With the two correction factors

$$k_T^* \approx \left(\frac{T_{aw}}{T_w} \right)^{0.2 \dots 0.4}$$

And

(8)

4.3 Cooling Efficiency According to Fogaroli and Saydah

Fogaroli and Saday used in their publication [28] a slightly different approach after Eq. (9):

$$\Theta = \frac{T_{r,g} - T_w}{T_{r,g} - T_c} = 1 - \frac{1}{1 + \frac{c_{p,c}}{c_{p,g}} \frac{F}{St_{g,0}} \frac{1}{\left[\left(\frac{F}{2St_{g,0}} \right)^2 + 1 \right]^{0.5}} - \frac{F}{2St_{g,0}}}}$$

(9)

4.4 Cooling Efficiency According to Bartle and Leadon

The cooling model of Bartle and Leadon [29] calculates the cooling efficiency by using Eq. (10):

$$\Theta = \frac{T_{r,g} - T_w}{T_{r,g} - T_c} = 1 - \frac{1}{\left(1 + \frac{1}{3} \frac{c_{p,c}}{c_{p,g}} \frac{F}{St_{g,0}} \right)^3}$$

(10)

4.5 Cooling Efficiency According to Kays et al.

Kays et al. [30] developed the approach of Eq. (11).

$$\Theta = \frac{T_{r,g} - T_w}{T_{r,g} - T_c} = 1 - \frac{1}{1 + \left(\frac{c_{p,c}}{c_{p,g}} \right)^{0.4} \left[\exp \left(\frac{F}{St_{g,0}} \left(\frac{c_{p,c}}{c_{p,g}} \right)^{0.6} \right) - 1 \right]}$$

(11)

4.6 Cooling Efficiency According to Rannie

One of the most common cooling efficiency estimations was developed by Rannie [31] and is given in Eq. (12).

$$\Theta = \frac{T_{r,g} - T_w}{T_{r,g} - T_c} = 1 - \frac{\exp(-36.9 Re_L^{0.1} Pr_g F)}{1 + \frac{c_{p,c}}{c_{p,g}} (1.1775 Re_L^{0.1} - 1) (1 - \exp(-36.9 Re_L^{0.1} F))}$$

(12)

4.7 Cooling Efficiency According to Experimental Data

For the estimation of the cooling efficiency out of the gained experimental data, T_w was determined out of the mean value of the data obtained by the thermocouples “ST-01” to “ST-08”. A decision filter mechanism in the data analysis prevents unwanted effects of single runaway values on the mean value. Thus data were smoothed by a Savitzky-Golay Filter and values with more than 97.5% of the local maximum value were used to decide the

evaluation region. Afterwards the unfiltered data were used to obtain the mean wall temperature. The coolant temperature T_c was obtained by the thermocouple in the supply plenum, whereas the nozzle exit temperature T_e was calculated out of the measured flow data of the air vitiator (see [23] and [24] for details on this calculation method). In order to calculate the recovery temperature at the nozzle exit $T_{r,e}$, the nozzle exit Mach number Ma_e and the recovery factor $r_{turb,e}$ are needed. The recovery factor $r_{turb,e}$ was calculated out of the Prandtl number at the nozzle exit Pr_e using the correlation for a turbulent boundary layer (see Eq. (15)).

$$\Theta = \frac{T_{r,e} - T_w}{T_{r,e} - T_c} \quad (13)$$

$$T_{r,e} = T_e \left(1 + r_{turb,e} \frac{(\kappa - 1)}{2} Ma_e^2 \right) \quad (14)$$

$$r_{turb,e} = (Pr_e)^{1/3} \quad (15)$$

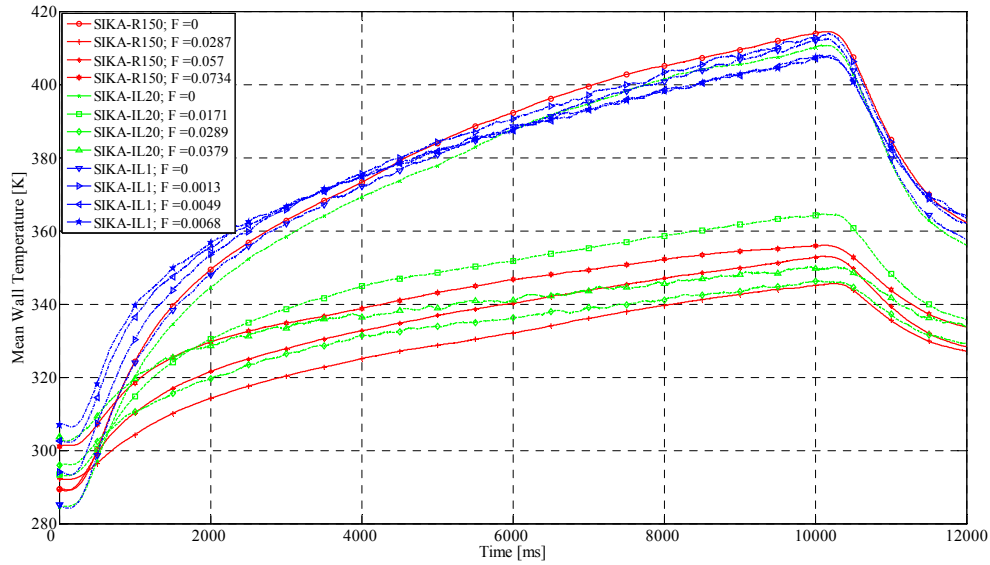


Figure 6: Mean Wall Temperature, 900 K, 10 bar without Shock Generator

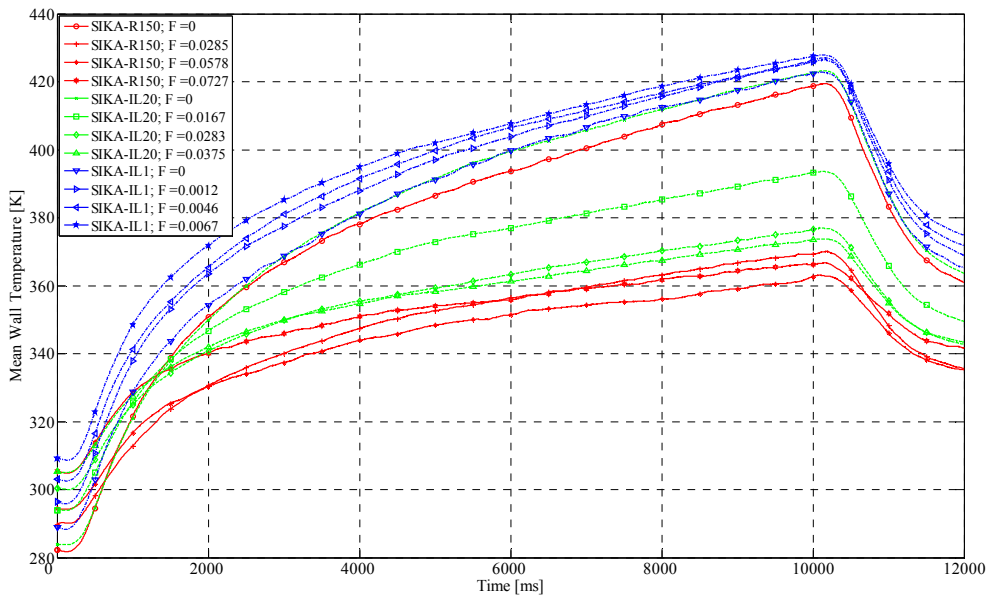


Figure 7: Mean Wall Temperature, 900 K, 10 bar with Shock Generator

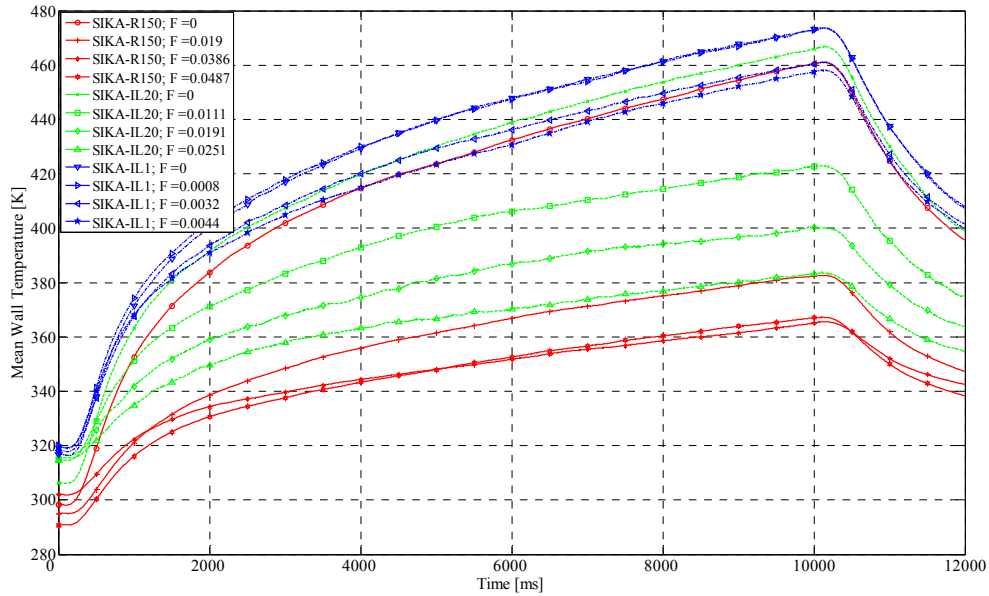


Figure 8: Mean Wall Temperature, 900 K, 15 bar without Shock Generator

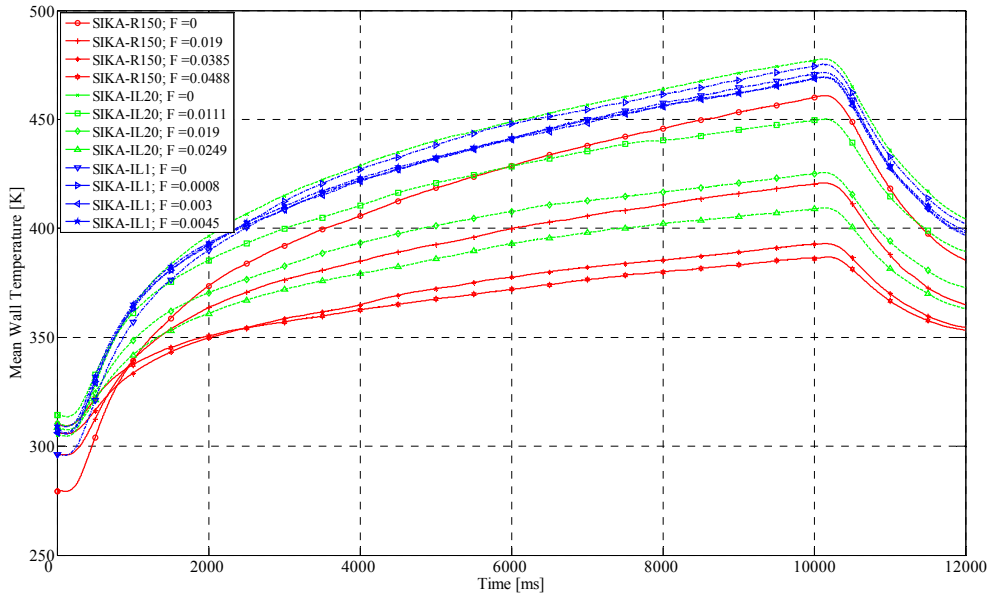


Figure 9: Mean Wall Temperature, 900 K, 15 bar with Shock Generator

In Fig. 6 the mean wall temperature profile is plotted against the testing time for different porous materials in testing configuration 1 (without shock generator) for the boundary stagnation conditions 900K and 10 bar. The maximum mean wall temperature can be decreased by about 80 K by the cooling system for a blowing ratio of 7.3%. However, if Sika-IL 20 is used, a blowing ratio of 3.8% is sufficient to reach a similar cooling effect. Small blowing ratios like they are provided by Sika-IL 1 have only small effect on the mean wall temperature.

If the shock generator is introduced in the model combustion chamber (testing configuration 2), the mixing between hot gas main flow and secondary coolant flow increases (see Fig. 7). This leads to a lower cooling performance compared to the case without shock generator and decreases the cooling effect to about 55 K temperature difference. Furthermore, the effect of smaller blowing ratios being nearly as effective as higher ones, if a different material is used, decreases under the influence of the shock generator.

A higher air vitiator mass flow (see Tab. 1) increases the mean wall temperature and in the 900 K / 15 bar case also the cooling performance of the transpiration cooling system whilst using smaller blowing ratios (see Fig. 8). If Fig. 8 and Fig. 9 are compared, it is clearly visible that like in the previous case for 900 K and 10 bar, the effect of similar performance at lower blowing ratios with Sika-IL 20 decreases. A reason for this could be that higher blowing ratios are necessary with the impinging shock to inject coolant deeper into the main flow whilst reducing the mean wall temperature in the mixed state downstream.

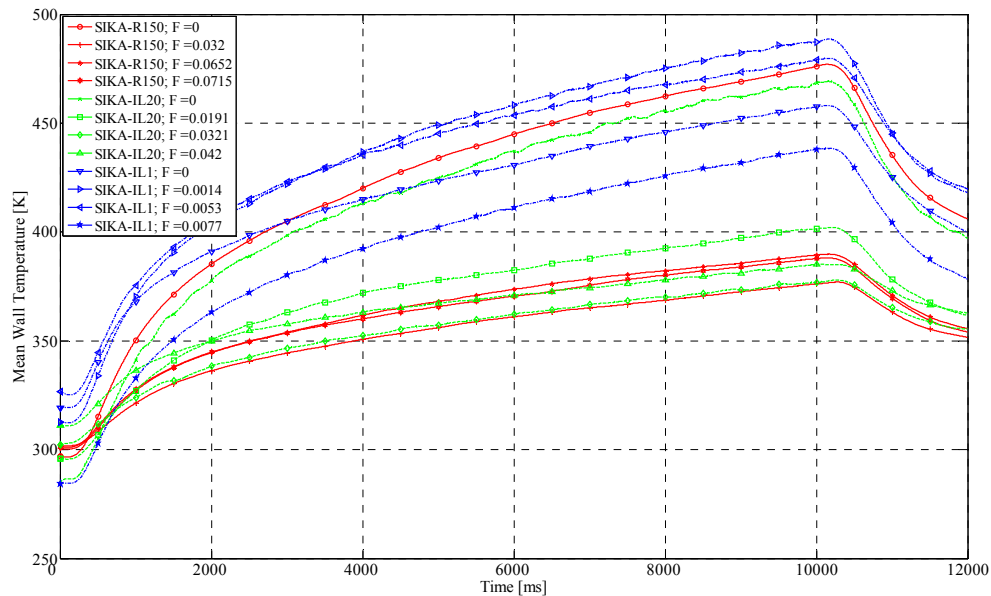


Figure 10: Mean Wall Temperature, 1200 K, 10 bar without Shock Generator

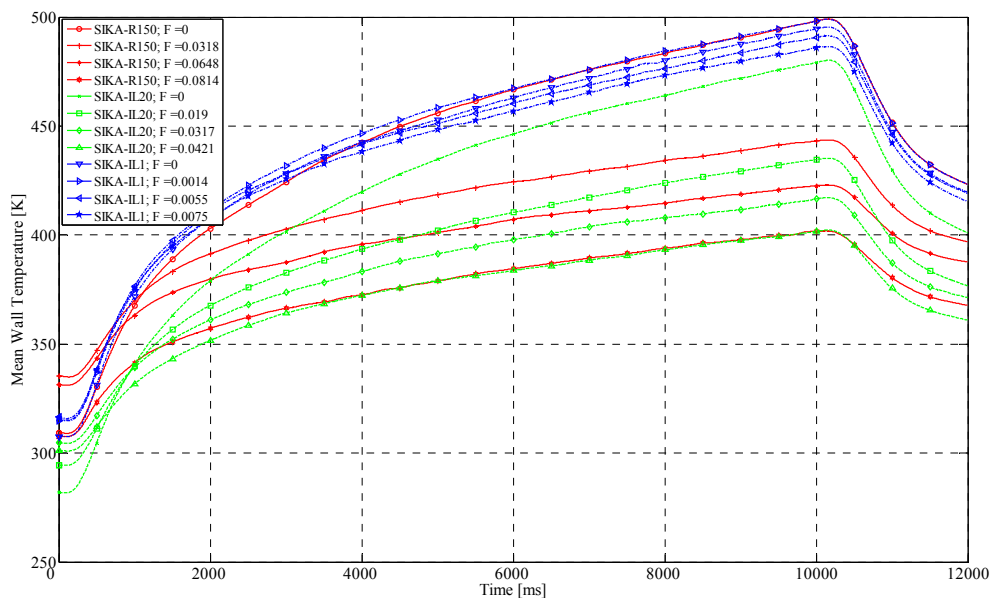


Figure 11: Mean Wall Temperature, 1200 K, 10 bar with Shock Generator

In Fig. 10 the mean wall temperature profile is displayed versus the testing time for different porous materials in testing configuration 1 (without shock generator) for the boundary stagnation conditions 1200K and 10 bar. It is obvious that the wall temperature downstream of the porous section is significantly lowered by the use of a transpiration cooling system. Low porosities (Sika-IL 1) result in low blowing ratios with less cooling effect on the wall. High porosities (Sika-R 150) are causing a higher cooling effect by higher blowing ratios.

However, in the area between 3% and 6% blowing ratio, a higher coolant mass flow causes only a small improvement of the cooling. It can also be observed that a similar cooling effect can be reached between Sika-IL 20 in the area of 3% to 4% blowing ratio compared with Sika-R 150 at 6% to 7% blowing ratio.

In Fig. 11 the same boundary conditions are displayed for testing configuration 2 (with shock generator). It is obvious that the temperature difference between the two cases with and without shock generator is similar for this testing condition. However, in case of the shock generator a higher blowing ratio is required to create a cooling effect downstream of the porous section.

At higher hot gas mass flow rates (see Fig. 12) the cooling effect of the transpiration cooling system increases downstream of the porous section. The wall temperature also decreases to the same cooled temperature by using a lower blowing ratio than in the 10 bar case. There is also a zone (2% to 4%), where an increase of the blowing ratio does not affect the wall temperature proportionally. A comparison with Fig. 13 shows the effect of the shock generator. With an increased main mass flow, a higher blowing ratio is required to gain a cooling effect. Additionally, the wall temperature with high cooling is higher than in the case without the shock generator.

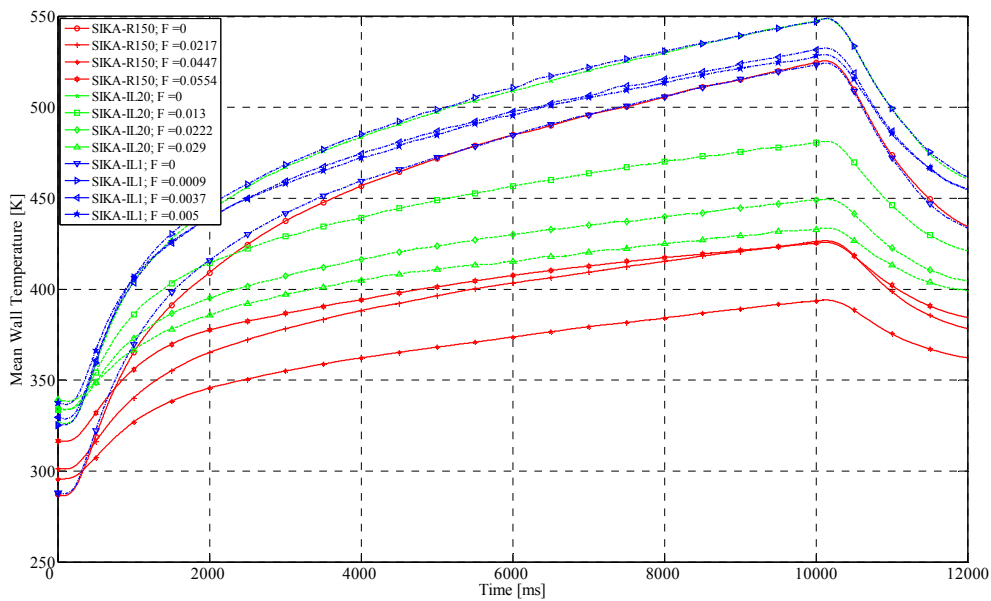


Figure 12: Mean Wall Temperature, 1200 K, 15 bar without Shock Generator

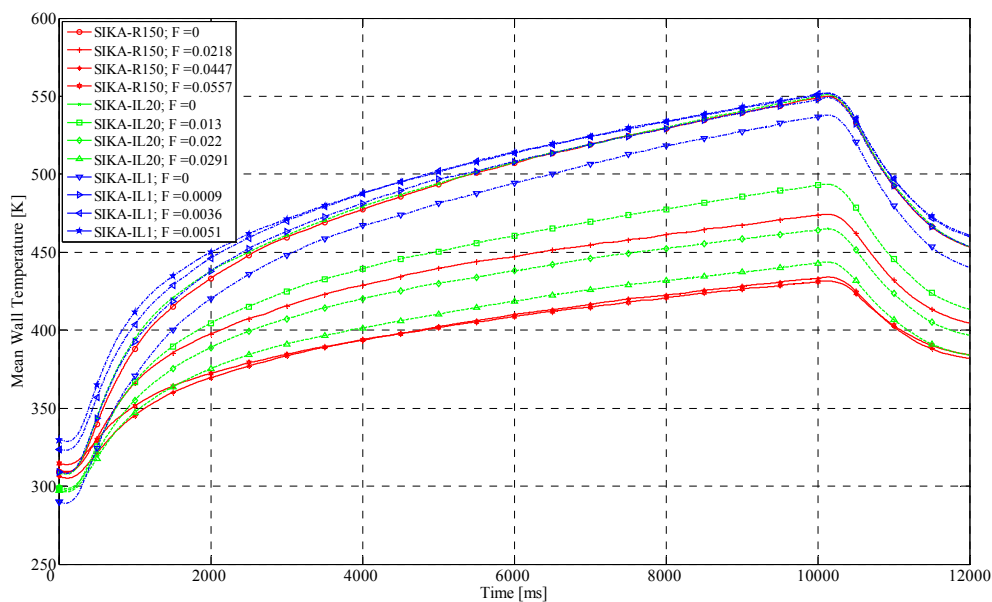


Figure 13: Mean Wall Temperature, 1200 K, 15 bar with Shock Generator

Small porosities (Sika-IL 1) have, again, less effect on the wall temperature, since they result in small blowing ratios. As in the 10 bar case, similar cooling performance can be reached with smaller porosities and smaller blowing ratios, if the porosities are not chosen too small.

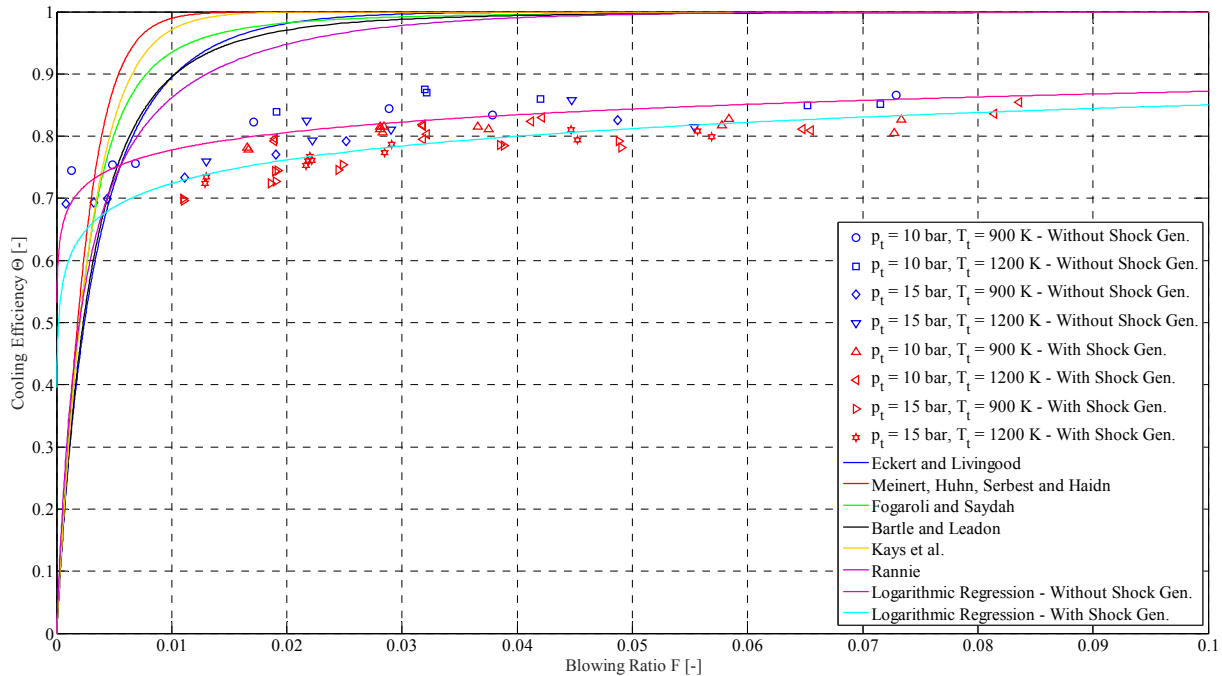


Figure 14: Cooling Efficiency vs. Blowing Ratio (Models and Experimental Data)

Fig. 14 displays the cooling efficiency for the experiments of this publication vs. the blowing ratio. Furthermore the used theoretical cooling models are shown for comparison. If all the experiments are analysed by a logarithmic regression, it can be shown that the introduction of a shock generator affects the cooling efficiency of the system. In general, smaller blowing ratios between 1% and 3% are affected slightly more by the shock generator than higher ones concerning in terms of cooling efficiency.

However, the theoretical cooling models for transpiration cooling systems differ about 15 to 25% compared to the experimental results. For higher blowing ratios (3% and more) the models trend to 100%, whereas the experimental results trend to 80 / 85% cooling efficiency. A general overestimation of the cooling efficiency by the cooling models and their limitation to small blowing ratios has been already recognized by other authors (see e.g. reference [14]). However the overestimation in reference [14] was smaller than in the experiments of the work at hand, since Langener used lower blowing ratios. The main reason for the stronger deviation of our experimental cooling efficiency is expected to be that the measurement region is positioned 25 mm downstream of the porous wall section. In this region hot gas from the main flow and cooler coolant has already mixed to a certain extend. This is expected to result in a higher wall temperature than if it would be measured directly at the surface of the porous sample. According to Eq. 13 a higher wall temperature causes a lower cooling efficiency. Additional experiments in the future and comparison with the temperatures measured closer to the porous wall (“ST-10”, “ST-12” and “ST-14” in configuration 3, see Fig. 5) will deeper investigate the cause for this discrepancy.

In general all results obtained in this work are not representing steady state conditions. Due to technical constraints (gas supplies and thermal load on air vitiator) it is not possible to run the test bench long enough to reach real steady state conditions or even thermal equilibrium. Therefore the applied testing time of ten seconds offers just a snapshot of the cooling process. However, the air vitiator reaches near steady state conditions already about two seconds after ignition (see [23] and [24]). Accordingly, the experimental results gained after two seconds of testing time were obtained under near steady state boundary conditions at the inlet of the scramjet model combustion chamber. Due to the mentioned limitations the results of the work at hand cannot be applied on scramjet engine or model combustion chamber durability analysis, but offer insights of the arising phenomena and processes.

5. Uncertainty Analysis

For every test run the random uncertainty of the mean $P_{\bar{x}}$ was calculated for the thermocouples after Eq. 16 (see [32]). In Eq. 16 S_x indicates the standard deviation and n is the number of measurements used for determining the average.

$$P_{\bar{x}} = 2 \frac{S_x}{n^{0.5}} \quad (16)$$

For Fig. 6 and Fig. 7 the worst case value for $P_{\bar{x}}$ was 1.62 K, for Fig. 8 and Fig. 9 1.84 K, for Fig. 10 and Fig. 11 2.28 K and for Fig. 12 and Fig. 13 2.54 K. Assuming a systematic uncertainty of the thermocouples of (0.0075*measured temperature value) according to the manufacturer, the maximum total uncertainties are calculated to 3.61 K for Fig. 6 and Fig. 7, 3.98 K for Fig. 8 and Fig. 9, 4.39 K for Fig. 10 and Fig. 11 and 4.84 K for Fig. 12 and Fig. 13.

The coolant temperature T_c is as a worst case assumed to have a similar uncertainty, since it is measured by one single type K thermocouple. The nozzle exit temperature T_e is calculated via the stagnation pressure T_t . The stagnation pressure is determined via the pressure measurement and the velocity calculation in the air vitiator. The highest random uncertainty of the mean value in the pressure measurement was 0.065 bar for 15 bar stagnation pressure and 0.040 bar for 10 bar stagnation pressure. This causes a calculation uncertainty of about 0.4% or 2.2 K of T_e in the worst case. In summary the uncertainty of the cooling efficiency caused by measurement uncertainties is determined to below 2%.

6. Conclusion

DLR Lampoldshausen has conducted experiments on the applicability of transpiration cooling systems in supersonic combustion ramjets. Gaseous nitrogen was used as coolant together with three different porous wall materials made of sintered stainless steel. Results were presented for 96 different blowing ratios. The results presented show that all usual models for the estimation of the cooling efficiency are overestimating the real cooling efficiency. This is particularly the case, if the cooling efficiency of the film caused by a transpiration cooling system is analysed some millimetres downstream of the porous wall section and / or high blowing ratios are used at the Mach number chosen. The 9.3° turning angle half wedge used as a shock generator in the experiments increased the mixing between hot gas main flow and the secondary coolant flow, but in general did not affect the transpiration cooling performance strongly. However, local hotspots especially in the uncooled case can still lead to structural damage on the combustion chamber wall, since the temperature can be increased locally by the impinging shock. Furthermore, in the cases with shock generator, a lower blowing ratio together with lower porosities could be used to reach a similar cooling effect. But it has to be taken into account that smaller blowing ratios generally cause a smaller cooling efficiency, which is more affected due to increased mixing if a shock generator is present.

7. Outlook

Further experiments have already been conducted using C / C fibre reinforced ceramics of different thicknesses and nitrogen as coolant. The results of those experiments will be part of future publications by the authors. At present, extensive tests with gaseous hydrogen as coolant for comparison are ongoing additionally. Results and comparisons with the experiments presented in the work at hand will also be part of additional publications. It has to be clarified in the future if the observed effects are also valid for different coolants or other porous materials. Additionally, tests with increased testing time will be performed to investigate its influence on the wall temperature distribution. Also a detailed analysis of the reason for the discrepancy between experimental data and common theoretical cooling models is planned.

Acknowledgements

The authors want to thank the staff of test bench M11 at the site of Lampoldshausen, especially Jan Witte, Lukas Werling, Hagen Friedrich, Jan Buddenberg and Marius Wilhelm.

References

- [1] Curran, E. and S. Murthy. 2000. Supersonic Flow Combustors. *Scramjet Propulsion, Progress in Astronautics and Aeronautics*. Vol. 189: 513-568.
- [2] Holden, M., Nowak, R., Olsen, G. and K. Rodriguez. 1990. Experimental Studies of Shock Wave/Wall Jet Interaction in Hypersonic Flow. AIAA 90-0607. American Institute of Aeronautics and Astronautics.
- [3] Holden, M. and S. Sweet. 1994. Studies of Transpiration Cooling With Shock Interaction in Hypersonic Flow. AIAA 94-2475. American Institute of Aeronautics and Astronautics.
- [4] Olsen, G. and R. Nowak. 1995. Hydrogen Film Cooling With Incident and Swept-Shock Interactions in a Mach 6.4 Nitrogen Free Stream. NASA Technical Memorandum 4603. National Aeronautics and Space Administration.
- [5] Meinert, J. 2000. Static Friction And Heat Transfer in a Turbulent Boundary Layer During Foreign Gas Transpiration. PhD Thesis. University of Dresden, VDI Reihe 7, Nr. 402, ISBN 3-18-340207-6. (In German).
- [6] Serbest, E. 2002. Investigations on Applicability of Effusion Cooling in Rocket Combustion Chambers. PhD Thesis, RWTH Aachen, Faculty of Mechanical Engineering. Shaker Verlag. ISBN 3-8322-0219-6. (In German).
- [7] Serbest, E. and O. Haidn. 1999. Effusion Cooling in Rocket Combustors Applying Fibre Reinforced Ceramics. AIAA 99-2911. American Institute of Aeronautics and Astronautics.
- [8] Meinert, J., Huhn, J., Serbest, E. and O. Haidn. 2000. Investigations on the Effect of Foreign Gas Transpiration on a Turbulent Boundary Layer. AIAA 2000-3386. American Institute of Aeronautics and Astronautics.
- [9] Meinert, J., Huhn, J., Serbest, E. and O. Haidn. 2001. Turbulent Boundary Layers with Foreign Gas Transpiration. *Journal of Spacecraft and Rockets*. Vol. 38, No. 2: 191-198.
- [10] Lezuo, M. and O. Haidn. 1997. Transpiration Cooling Using Gaseous Hydrogen. AIAA 1997-2909. American Institute of Aeronautics and Astronautics.
- [11] Lezuo, M. and O. Haidn. 1996. Transpiration Cooling in H₂ / O₂-combustion Devices. AIAA 96-2581. American Institute of Aeronautics and Astronautics.
- [12] Lezuo, M. 1998. Heat Transfer in H₂ Transpiration Cooled Combustion Chamber Components. PhD Thesis, RWTH Aachen, Faculty of Mechanical Engineering. Shaker Verlag. ISBN 3-8265-4481-1. (In German).
- [13] Greuel, D. 2013. Investigations on Momentum and Mass Transport in Effusion Cooled Rocket Combustion Chamber Walls Made of Fibre Ceramics. PhD Thesis. RWTH Aachen, Faculty of Mechanical Engineering. (In German).
- [14] Langener, T. 2011. A Contribution to Transpiration Cooling for Aerospace Applications Using CMC Walls. PhD Thesis. University of Stuttgart, Faculty of Aerospace Engineering and Geodesy.
- [15] Song, K., Choi, S. and S. Scotti. 2006. Transpiration Cooling Experiment for Scramjet Engine Combustion Chamber by High Heat Fluxes. *Journal of Propulsion and Power*. Vol. 22, No. 1: 96-102.
- [16] Olsen, G., Holden, M. and N. Baker. 1990. Experimental Results for Film Cooling in 2-D Supersonic Flow Including Coolant Delivery Pressure, Geometry, and Incident Shock Effects. AIAA 90-605. American Institute of Aeronautics and Astronautics.
- [17] Juhany, K. and M. Hunt. 1994. Flowfield Measurements in Supersonic Film Cooling Including the Effect of Shock-Wave Interaction. *AIAA Journal*. Vol. 32, No.3: 578-585.
- [18] Menon, S. 1989. Shock-Wave-Induced Mixing Enhancement in Scramjet Combustors. AIAA 89-0104. American Institute of Aeronautics and Astronautics.
- [19] Alzner, E. and V. Zakkay. 1970. Turbulent Boundary Layer Shock Interaction With and Without Injection. AIAA 70-91. American Institute of Aeronautics and Astronautics.
- [20] Gerlinger, P. and D. Brüggemann. 2000. Numerical Investigation of Hydrogen Strut Injections into Supersonic Airflows. *Journal of Propulsion and Power*. Vol. 16, No. 1: 22-28.
- [21] Peng, W. and P. Jiang. 2009. Influence of Shock Waves on Supersonic Film Cooling. *Journal of Spacecraft and Rockets*. Vol. 46, No. 1: 67-73.
- [22] Goldstein, R., Eckert, E. and D. Wilson. 1968. Film Cooling With Normal Injection into Supersonic Flow. *Transactions of the ASME, Journal of Engineering for Industry*. Vol. 90, No. 4: 584-588.
- [23] Strauss, F., Manfletti, C., Lieberwirth, R. and S. Schlechtriem. 2016. Experimental Setup on Transpiration Cooling in Supersonic Combustion Ramjets (Scramjets). SP2016_3125033, *Space Propulsion Conference 2016, 02-06th May 2016, Roma*.
- [24] Strauss, F., Manfletti, C., Freudenmann, D., Witte, J. and S. Schlechtriem. 2016. Preliminary Experiments on Transpiration Cooling in Ramjets and Scramjets. AIAA 2016-4968. American Institute of Aeronautics and Astronautics.
- [25] Weisgerber, H., Martinuzzi, R., Brummund, U. and Ph. Magre. 2001. PIV Measurements in a Mach 2 Hydrogen-Air Supersonic Combustor. AIAA 2001-1757. American Institute of Aeronautics and Astronautics.
- [26] Settles, G. 2001. *Schlieren and Shadowgraph Techniques*. 1st Edition. Springer-Verlag. pp.39-48.

- [27] Eckert, E. and J. Livingood. 1954. Comparison of Effectiveness of Convection-, Transpiration-, and Film-Cooling Methods with Air as Coolant. Report 1182. National Advisory Committee for Aeronautics (NACA), Lewis Flight Propulsion Laboratory, Cleveland, OH.
- [28] Fogaroli, R. and A. Saydah. 1966. Turbulent Heat Transfer and Skin Friction Measurements on a Porous Cone With Air Injection. *AIAA Journal*. Vol. 4, No. 6 : 1116-1117.
- [29] Bartle, E. and M. Leadon. 1959. Experimental Evaluation of Heat Transfer with Transpiration Cooling in a Turbulent Boundary Layer at $M=3.2$. *Journal of the Aerospace Sciences*. Vol. 26 : 78-80.
- [30] Kays, W., Crawford, M. and B. Weigand. 2005. *Convective Heat and Mass Transfer*. 4th Edition. McGraw-Hill.
- [31] Rannie, W. 1947. A Simplified Theory of Porous Wall Cooling. Technical Report. Jet Propulsion Laboratory, Pasadena.
- [32] Wheeler, J. and A. Ganji. 2010. *Introduction to Engineering Experimentation*. 3rd Edition. Pearson. pp.206-207.